CANCER BIOTHERAPY AND RADIOPHARMACEUTICALS
Volume 24, Number 4, 2009

DOI: 10.1089/cbr.2009.0674

Copper-64 Radiopharmaceuticals for PET Imaging of Cancer: Advances in Preclinical and Clinical Research

Carolyn J. Anderson[1–3] and Riccardo Ferdani[1]

Summation

Copper-64 ($T_{1/2} = 12.7$ hours; β^+, 0.653 MeV [17.8 %]; β^-, 0.579 MeV [38.4 %]) has decay characteristics that allow for positron emission tomography (PET) imaging and targeted radiotherapy of cancer. The well-established coordination chemistry of copper allows for its reaction with a wide variety of chelator systems that can potentially be linked to peptides and other biologically relevant small molecules, antibodies, proteins, and nanoparticles. The 12.7-hours half-life of ^{64}Cu provides the flexibility to image both smaller molecules and larger, slower clearing proteins and nanoparticles. In a practical sense, the radionuclide or the ^{64}Cu-radiopharmaceuticals can be easily shipped for PET imaging studies at sites remote to the production facility. Due to the versatility of ^{64}Cu, there has been an abundance of novel research in this area over the past 20 years, primarily in the area of PET imaging, but also for the targeted radiotherapy of cancer. The biologic activity of the hypoxia imaging agent, $^{60/64}$Cu-ATSM, has been described in great detail in animal models and in clinical PET studies. An investigational new drug application for ^{64}Cu-ATSM was recently approved by the U.S. Food and Drug Administration (FDA) in the United States, paving the way for a multicenter trial to validate the utility of this agent, with the hopeful result being FDA approval for routine clinical use. This article discusses state-of-the-art cancer imaging with ^{64}Cu radiopharmaceuticals, including ^{64}Cu-ATSM for imaging hypoxia, ^{64}Cu-labeled peptides for tumor-receptor targeting, ^{64}Cu-labeled monoclonal antibodies for targeting tumor antigens, and ^{64}Cu-labeled nanoparticles for cancer targeting. The emphasis of this article will be on the new scientific discoveries involving ^{64}Cu radiopharmaceuticals, as well as the translation of these into human studies.

Key words: antibody, bone metastastes, cancer, PET, molecular imaging

Introduction

A significant research effort has been devoted to the copper radionuclides because they offer a varying range of half-lives and positron energies (Table 1). In addition, the well-established coordination chemistry of copper allows for its reaction with a wide variety of chelator systems that can be linked to antibodies, proteins, peptides, and other biologically relevant small molecules. This update will focus on ^{64}Cu radiopharmaceuticals for positron emission tomography (PET) imaging applications. The longer half-life allows ^{64}Cu to be produced at regional or national cyclotron facilities and distributed to local nuclear medicine departments with the loss of approximately one half-life. In addition, the longer half-life is compatible with the time scales required for the optimal biodistribution of slower clearing agents, such as monoclonal antibodies (mAbs), nanoparticles, and higher molecular weight polypeptides requiring longer imaging times.

Production of Copper Radionuclides

The production of no-carrier-added ^{64}Cu via the ^{64}Ni(p,n)^{64}Cu reaction on a biomedical cyclotron was proposed by Szelecsenyi et al. In this study, small irradiations were performed demonstrating the feasibility of ^{64}Cu production

[1]Mallinckrodt Institute of Radiology, [2]Department of Biochemistry and Molecular Biophysics, and [3]Department of Chemistry, Washington University School of Medicine, St. Louis, Missouri.

Address correspondence to: Carolyn J. Anderson; Mallinckrodt Institute of Radiology, 510 Street, Kingshighway Boulevard, Campus Box 8225, St. Louis, MO 63110
E-mail: **andersoncj@mir.wustl.edu**

Table 1. Decay Characteristics of Copper Radionuclides

Isotope	$t_{1/2}$	β^- *MeV (%)*	β^+ *MeV (%)*	*EC (%)*	γ *MeV (%)*
^{60}Cu	23.4 minutes	—	2.00 (69) 3.00 (18) 3.92 (6)	7.0	0.511 (186) 0.85 (15) 1.33 (80) 1.76 (52) 2.13 (6)
^{61}Cu	3.32 hours	—	1.22 (60%)	40	0.284 (12) 0.38 (3) 0.511 (120)
^{62}Cu	9.76 minutes	—	2.91 (97%)	2	0.511 (194)
^{64}Cu	12.7 hours	0.573 (38.4)	0.655 (17.8%)	43.8	0.511 (35.6) 1.35 (0.6)
^{67}Cu	62.0 hours	0.395 (45) 0.484 (35) 0.577 (20)	—	—	0.184 (40)

by this method.[1] At present, the most common production method for ^{64}Cu utilizes the ^{64}Ni(p,n)^{64}Cu reaction,[1–4] which involves the irradiation of enriched ^{64}Ni that has been electroplated on a gold[1,2,4,5] or rhodium platform.[6] McCarthy et al. have described the efficient production of high-specific-activity ^{64}Cu by using a small biomedical cyclotron and a ^{64}Ni-enriched (>95%) target.[2] The ^{64}Ni(p,n)^{64}Cu transmutation reaction is high yielding (2.3–5.0 mCi h^{-1}), and after purification by using an ion-exchange column, high-specific-activity samples of [^{64}Cu]-$CuCl_{2g}$ were obtained (95–310 mCi μg^{-1}). Obata et al., reported yields of 0.6– >3.0 mCi/μAh, averaging 1.983 mCi/μAh with a radionuclidic purity of over 99% with using a 12 MeV cyclotron,[4] while Avila-Rodriguez et al. improved yields to >7 mCi/μAh with 11.4-MeV protons.[7] Using a tangential target on the National Institutes of Health (NIH) CS-30 cyclotron, Szajek et al., reported yields of 10.5 ± 3 mCi/μAh when bombarded with a 12.5-MeV proton beam, which was comparable to the theoretic yield, and over 3 hours produced >1 Ci of radioactivity.[8] The use of ^{64}Cu has dramatically increased in the past decade[9] and its production and has now been reported by academic sources in the United States,[2,8] Europe,[6] and Japan.[4]

Coordination Chemistry of Copper(II)

The aqueous-solution coordination chemistry of copper is limited to three oxidation states (I–III).[10–12] Due to the lability of most Cu(I) complexes, they typically lack sufficient kinetic stability for radiopharmaceutical applications, while Cu(III) is relatively rare and difficult to attain without the use of strong π-donating ligands. Copper (II) is a d^9 metal of borderline softness, which favors amines, imines, and bidentate ligands, such as bipyridine to form square planar, distorted square planar, trigonal pyramidal, square pyramidal, as well as distorted octahedral geometries. Cu(II) is generally less labile toward ligand exchange and is the best candidate for incorporation into radiopharmaceuticals. Jahn-Teller distortions in six-coordinate Cu(II) complexes are often observed as an axial elongation or a tetragonal compression. Although Cu(II) is less labile than Cu(I) and ^{64}Cu is a good radionuclide for PET imaging, the kinetic stability of Cu(II) complexes *in vivo* is very different from the thermodynamic stability in aqueous solution. Therefore, the development of Cu(II) complexes for radiopharmaceutical applications has been an active area of research.

Chelators based on cyclam and cyclen backbones

The most widely used chelators for attaching ^{64}Cu to biologic molecules are tetraazamacrocyclic ligands with pendant arms that utilize both the macrocyclic and chelate effects to enhance stability. By far, the most extensively used class of chelators for ^{64}Cu has been the macrocyclic polyaminocarboxylates shown in Figure 1. Two of the most widely studied chelators are DOTA (1,4,7,10-tetraazacyclododecane-1,4,7,10-tetraacetic acid) and TETA (1,4,8,11-tetraazacyclotetradecane-1,4,8,11-tetraacetic acid). While DOTA has been used as a BFC (bifunctional chelator) for ^{64}Cu, its ability to bind many different metal ions and its decreased stability, compared to TETA, make it less than ideal.[13–18] The tetraazamacrocyclic ligand, TETA, therefore, has been extensively used as a chelator for ^{64}Cu, and successful derivatization of this ligand has allowed researchers to conjugate it to antibodies, proteins, and peptides.[19–26]

Although ^{64}Cu-TETA complexes are more stable than ^{64}Cu-DOTA and ^{64}Cu-labeled complexes of acyclic ligands, their instability *in vivo* has been well documented by our lab. Bass et al. demonstrated that when ^{64}Cu-TETA-octreotide (OC) was injected into normal Sprague-Dawley rats, nearly 70% of the ^{64}Cu from ^{64}Cu-TETA-OC was transchelated to a 35-kDa species believed to be superoxide dismutase (SOD) in the liver 20 hour postinjection.[27] These results are supported by the observations of Boswell et al.[28]

Sarcophogine chelators

Another class of ligands that has gained attention as potential ^{64}Cu chelators are the hexaazamacrobicyclic cage-type ligands, which are based upon the sepulchrate or sarcophagine cage motifs (Fig. 1) and whose syntheses were first described by Sargeson.[29] Both cage systems are synthesized by reaction of the inert tris-ethylenediamine cobalt (III) complex with formaldehyde, followed by reaction with ammonia/formaldehyde or nitromethane/formaldehyde under basic conditions to generate the sepulchrate or sarcophagine (Sar) ligands, respectively. Smith et al. investigated a family of Sar

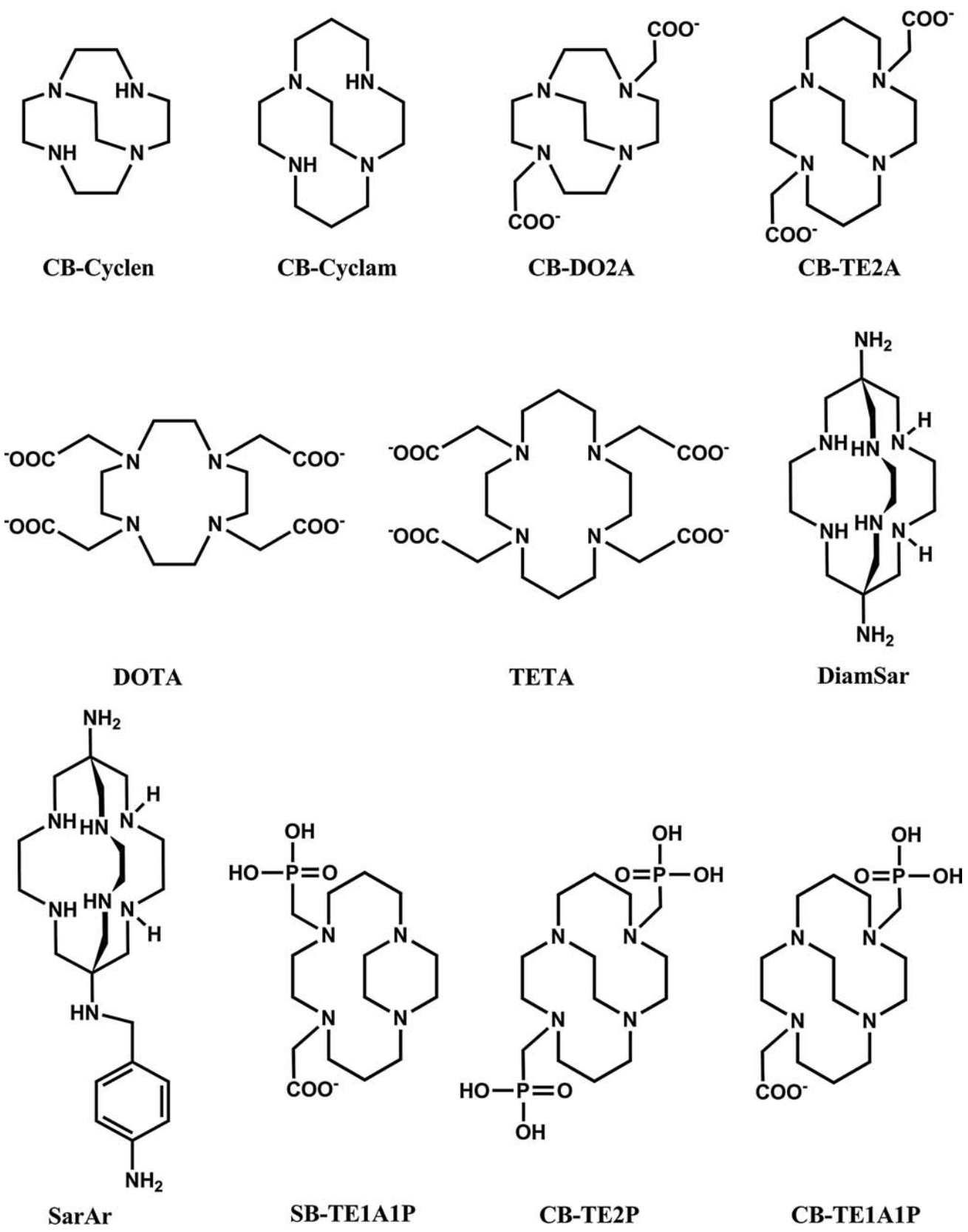

FIG. 1. Structures of macrocyclic chelators for complexing copper radionuclides.

derivatives with various functional groups at the apical sites, while the SarAr ligand was used to determine the ^{64}Cu complexation rates from pH 4 to 9.[30] From the data presented, complexation was 100% complete within several minutes at 25°C over the entire pH range. Biodistribution data was collected by using ^{64}Cu-Sar, ^{64}Cu-diamSar, and ^{64}Cu-SarAr in Balb/c mice. All three complexes cleared from the blood rapidly, and uptake was low in bone, heart, stomach, spleen, muscle, lungs, and the gastrointestinal tract. Liver clearance was observed to be good over the 30-minute time course of this study, demonstrating that the ^{64}Cu complexes are initially stable *in vivo*, but clearance of all three ^{64}Cu complexes is much slower through the kidney. Activity levels increased in the case of the ^{64}Cu-Sar complex, though this type of accumulation is not uncommon for positively charged complexes.

The cross-bridged tetraamine ligands

This class of chelators was first conceived of and synthesized by Weisman et al. in the 1990s,[31,32] and they were originally designed to complex metal cations, such as Li^+, Cu^{2+}, and Zn^{2+}, within their clamshell-like clefts. Numerous copper complexes of these and related ligands have since been prepared and studied by the Wong and Weisman labs as well as other research groups.[33–39] The expected *cis*-folded coordination geometry of these chelators has been confirmed in all cases via the available structural data. The attachment of two carboxymethyl pendant arms to CB-cyclam to give CB-TE2A (4,11-bis(carboxymethyl)-1,4,8,11-tetraazabicyclo[6.6.2]hexadecane) further ensures the complete envelopment of a six-coordinate Cu(II).

While the measurement of stability constants of Cu(II)-CB complexes have been limited by the proton-sponge nature of these chelators, available data for Cu(II)-CB-cyclam (log $K_f = 27.1$) revealed very similar values to nonbridged Cu(II)-cyclam (log $K_f = 27.2$) and related complexes.[40] On the other hand, their kinetic inertness, especially in aqueous solution, has been shown to be truly exceptional.[41,42] Proton-assisted decomplexation is one indicator of solution inertness. Under pseudo–first-order conditions of high-acid concentration (e.g., 5 M HCl), decomplexation half-lives can provide a comparative gauge. For example, Cu-CB-cyclam is almost 1 order of magnitude more inert than Cu (II)-cyclam in 5 M HCl at 90°C, while Cu(II)-CB-TE2A is 4 orders of magnitude more inert ($T_{1/2} = 154$ hour). Impressively, the latter complex resists acid decomplexation even better than the fully encapsulated sarcophagine complex, Cu(II)-diamsar (3,6,10,13,16,19-hexaazabicyclo[6.6.6]eicosane-1,8-diamine) ($T_{1/2} = 40$ hours).[43] It was confirmed that both the cross-bridged cyclam backbone as well as the presence of two enveloping carboxymethyl arms are required for this unusual kinetic inertness.

Biologic stability of ^{64}Cu-labeled cross-bridged complexes, including CB-cyclam, ^{64}Cu-CB-TE2A, and CB-DO2A (10-bis (carboxymethyl)-1,4,7,10-tetraazabicyclo[5.5.2]tetradecane), has been investigated.[28,40] The biodistribution of these ^{64}Cu complexes in female Sprague-Dawley rats were highly dependent upon the chelator. Based on the rapid clearance from the blood, liver, and kidney, ^{64}Cu-CB-TE2A was thought to be the most stable.[40] Follow-up metabolism studies of ^{64}Cu-CB-TE2A and ^{64}Cu-CB-DO2A, compared to ^{64}Cu-DOTA and ^{64}Cu-TETA, demonstrated the robust stability of ^{64}Cu-CB-TE2A *in vivo*, with low amounts of transchelation to the liver and blood proteins.[28]

In order to find chelators that complex Cu(II) with faster kinetics while retaining the high stability and the significant inertness observed with CB-TE2A, phosphonic-acid (-CH_2-PO_3H_2) donor groups were investigated as pendant arms.[44,45] It has been shown previously that chelators with phosphonic-acid pendant arms have higher selectivity as well as increased thermodynamic and kinetic stability, compared to their acetic acid analogs.[46] Cross-bridged 1,4,8,11-tetraazacyclotetradecane-1,8-bis(methanephosphonic acid) (CB-TE2P) and 4,8,11-tetraazacyclotetradecane-1-(methanephosphonic acid)-8-(methanecarboxylic acid) (CB-TE1A1P) were synthesized, radiolabeled with ^{64}Cu, and their *in vivo* behavior was investigated.[47] While CB-TE2P labeling with ^{64}Cu was complete within 1 hour in buffer at higher temperatures, radiolabeling yields above 90% were observed even at 37°C. CB-TE1A1P had 100% radiolabeling yields at 37°C. Preliminary biodistribution studies showed that the biodistribution of ^{64}Cu-CB-TE2P and ^{64}Cu-CB-TE1A1P compared favorably to ^{64}Cu-CB-TE2A.

Boswell et al. synthesized a side-bridged monophosphonate monoacid chelator, ((8-phosphonomethyl-1,5,8,12-tetraazabicyclo[10.2.2]hexadec-5-yl)-acetic acid (SB-TE1A1P)), and labeled it with ^{64}Cu.[48] This agent required radiolabeling conditions of 95°C, unlike the cross-bridged phosphonate chelators. Biodistribution in normal mice showed ^{64}Cu-SB-TE1A1P to be cleared rapidly through blood and other tissues, suggesting it is highly stable *in vivo*, similar to the cross-bridged chelators.

Imaging Tumor Hypoxia with $^{64/60}$Cu-ATSM

There is one class of copper radiopharmaceuticals where the stability of the Cu(II) complex is not essential for successful targeting. Cu(II) thiosemicarbazones have been evaluated as blood-flow agents and for imaging tumor hypoxia. In this article, we discuss the most recent developments for imaging tumor hypoxia with this class of agents.

It is well established that hypoxia is an important determinant of the overall response of the tumor to conventional therapy. The presence of hypoxia can result in an increase in tumor aggressiveness, failure of local control, and activation of transcription factors that support cell survival and migration.[49–51] The ability to locate and quantify the extent of hypoxia within solid tumors by using noninvasive nuclear imaging would facilitate early diagnosis and help clinicians select the most appropriate treatment for each individual patient.[50]

In 1997, Fujibayashi et al. discovered that the neutral, lipophilic copper(II) complex of the N_2S_2 tetradentate ligand, diacetyl-2,3-*bis*(N^4-methyl-3-thiosemicarbazone), commonly referred to as Cu-ATSM, showed hypoxia-selective uptake in *ex vivo* ischemic, perfused, isolated rat-heart models.[52,53] Cu-ATSM was later shown to be hypoxia selective *in vitro* and for tumor hypoxia.[52,54–59] Recent experimental and computational work provided the first experimental evidence directly probing the reduction, reoxidation, and pH-mediated ligand dissociation reactions of Cu-ATSM and their relationship to hypoxia selectivity.[58]

The thiosemicarbazones have been evaluated with the short-lived copper radionuclides, ^{60}Cu and ^{62}Cu ($T_{1/2} = 0.16$ hours, $\beta^+ = 98\%$, EC = 2%). Takahashi et al.[60] reported

the first human studies of the uptake of ^{62}Cu-ATSM in 10 patients: 4 normal patients and 6 with lung cancer. High tumor uptake was observed (uptake ratio, 3.00 ± 1.50) in all patients with lung cancer. Dehdashti et al. reported the first correlative studies comparing the uptake of ^{60}Cu-ATSM ($T_{1/2} = 0.16$ hour, $\beta^+ = 98\%$, EC = 2%) with response to conventional therapies in patients with non-small-cell lung cancer (NSCLC)[61] and cervical cancer.[62] In the NSCLC study, response to therapy was evaluated by using ^{60}Cu-ATSM tumor-to-muscle (T/M) uptake ratios. Imaging with [^{18}F]-FDG was also conducted as part of the routine clinical evaluation. Of the 14 patients studied, 8 responded to radiotherapy (5 showed a complete response with 3 partial responders) and 6 showed no response. The mean ^{60}Cu-ATSM T/M ratio of nonresponders (3.4 ± 0.8) was found to be much larger than uptake observed in responders (1.5 ± 0.4) [$p = 0.002$]. However, no significant differences were observed in the standardized uptake values (SUVs) between the tumors of responders (3.5 ± 1.0) and nonresponders (2.8 ± 1.1) [$p = 0.2$]. The threshold T/M value of 3.0 was identified as an accurate cut-off value for distinguishing responders from nonresponders. In contrast to the results with ^{60}Cu-ATSM, no significant differences were observed in either the mean T/M ratios or SUVs for the uptake of [^{18}F]-FDG (2-Fluoro-2-deoxy-D-glucose) in responders (12.7 ± 10.4) and nonresponders (10.9 ± 4.1) [$p = 0.7$]. In addition, no statistically significant correlation between ^{60}Cu-ATSM and [^{18}F]-FDG uptake was observed.

Before radiolabeled Cu-ATSM could be used for routine clinical analysis, accurate dosimetry measurements were required. In 2005, Laforest et al. used the Medical Internal Radionuclide Dose (MIRD) approach to provided estimates of human absorbed doses from $^{60/61/62/64}$Cu-ATSM by extrapolating data acquired from biodistribution data in rat models.[63] Calculated organ doses for ^{61}Cu, ^{62}Cu, and ^{64}Cu were extrapolated from the results obtained for ^{60}Cu-ATSM dosimetry. The estimated human dose for safe injection into an adult was predicted to lie between 500 and 800 MBq. Human doses using ^{64}Cu-ATSM have also been estimated from biodistribution data in non-tumor-bearing hamsters.[56]

Lewis et al. reported the first clinical comparison between the imaging characteristics of ^{60}Cu-ATSM and ^{64}Cu-ATSM (and [^{18}F]-FDG) in cancers of the uterine cervix conducted after Cu-ATSM was approved for study as an investigational new drug (IND 62,675) (Figure 2).[64] The study concluded that tumor uptake of Cu-ATSM as measured in images recorded between 1 and 9 days was reproducible, irrespective of the radionuclide used. This important result showed that Cu-ATSM is a marker for chronic tumor hypoxia, as opposed to acute hypoxia. Pretherapy imaging has also confirmed previous results indicating that the PET imaging of Cu-ATSM provides clinically relevant information about tumor oxygenation and is predictive of the likelihood of disease-free survival post-treatment in patients with cervical cancer.[65]

Copper-64-Labeled Somatostatin Analogs for Targeting Neuroendocrine Tumors

Somatostatin is a 14-amino-acid peptide that is involved in the regulation and release of a number of hormones, and somatostatin receptors (SSRs) are present in many different normal organ systems, such as the central nervous system (CNS), the gastrointestinal tract, and the exocrine and endocrine pancreas. Several human tumors of the neuroendocrine system, CNS, breast, and lung are SSR positive, making it a viable disease target. Further, the presence of SSRs in a tumor is predictive of a good therapeutic response. An 8-amino-acid analog of somatostatin, octreotide (OC) has a longer biologic half-life and is shown to be several times more effective than somatostatin in the suppression of growth-hormone secretion in animals.[66] Somatostatin analogs that have been conjugated with various metal chelators and labeled with ^{64}Cu for evaluating SSR-positive tumors in rodent models and humans are represented in Figure 3.

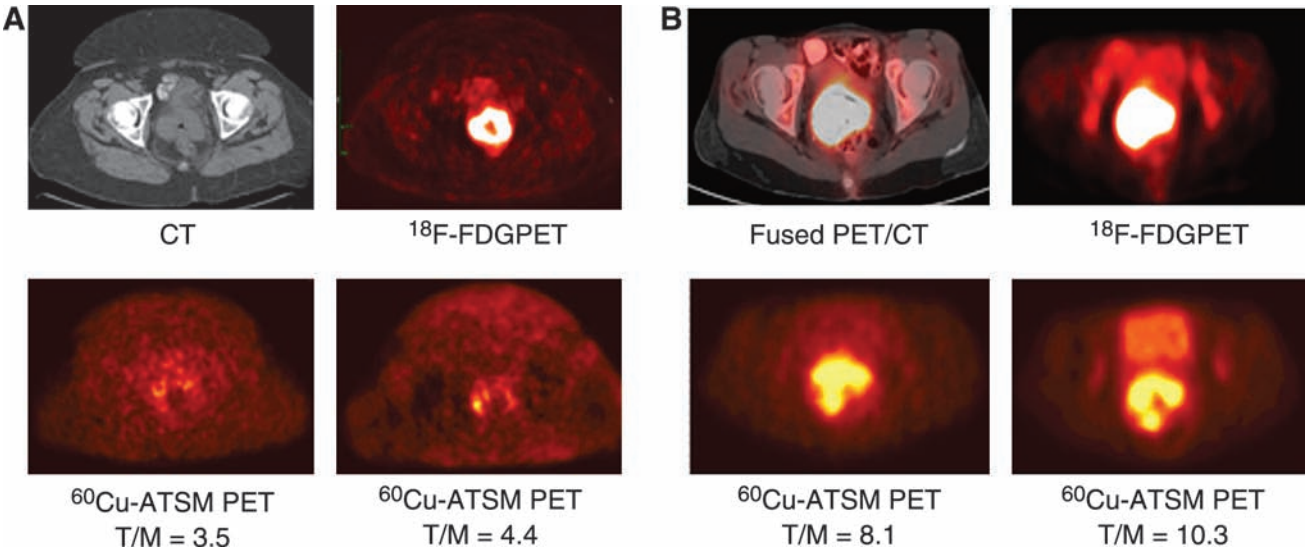

FIG. 2. Transaxial positron emission tomography/computed tomography (PET/CT) images showing the CT image (top left), [^{18}F]-FDG (Fluorine-18-2-fluoro-2-deoxy-D-glucose) image, ^{60}Cu-ATSM and ^{64}Cu-ATSM images recorded between 30 and 60 minutes in 2 patients with known cervical cancers. (**A**) Images recorded for a patient who responded to conventional radiotherapy and (**B**) images from a nonresponder. Reprinted by permission of the Society of Nuclear Medicine from reference 64.

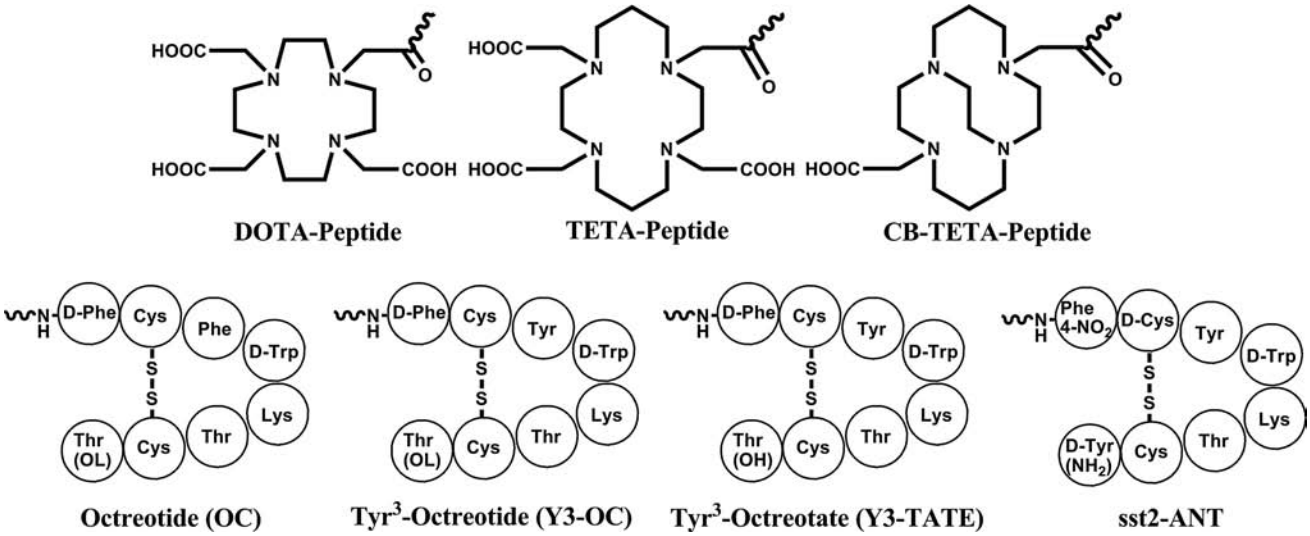

FIG. 3. Amino-acid sequences of somatostatin analogs used in imaging with ^{64}Cu and the chelators used to complex ^{64}Cu.

In one of earlier studies with SSRs, *in vitro* and *in vivo* evaluation of ^{64}Cu-labeled OC conjugates was performed.[20] OC was conjugated with TETA for labeling with ^{64}Cu, and this agent was compared with ^{111}In-DTPA-D-Phe^1-OC (^{111}In-DTPA-OC; Octreoscan,® Coviden, Hazelwood, MO), a single-positron emission computed tomography (SPECT) imaging agent approved for routine clinical use as a diagnostic agent for neuroendocrine cancer in the United States and Europe.[67] ^{64}Cu-TETA-OC was evaluated as a PET imaging agent in humans (8 subjects) and compared to ^{111}In-DTPA-OC with gamma scintigraphy and SPECT imaging.[22] ^{64}Cu-TETA-OC and PET imaged more tumors in 2 patients, compared to ^{111}In-DTPA-OC and SPECT, and in 1 patient, ^{111}In-DTPA-OC and SPECT weakly imaged a lung lesion that was not detected with ^{64}Cu-TETA-OC. Overall, ^{64}Cu-TETA-OC and PET showed greater sensitivity for imaging neuroendocrine tumors, in part due to the greater sensitivity of PET, compared to SPECT.

In vitro and *in vivo* evaluation of a second-generation somatostatin analog, ^{64}Cu-TETA-Y3-TATE (Y3-TATE: tyrosine-3-octreotate), were conducted, where Y3-TATE differs from OC in that tyrosine (Tyr) replaces phenylalanine (Phe) in the 3-position, and the *C*-terminal threonine (Thr) is an acid rather than an alcohol. Y3-TATE previously showed improved targeting of somatostatin-rich tissues.[24,68] ^{64}Cu-TETA-Y3-TATE had high binding affinity to somatostatin in receptor-positive rat pancreatic tumor-cell membranes, while in rat pancreatic tumor models, ^{64}Cu-TETA-Y3-TATE had twice as much uptake as ^{64}Cu-TETA-OC. This reagent demonstrated superior potential as a radiopharmaceutical for the imaging and therapy of SSR-positive tissues.

After demonstrating the superiority of CB-TE2A, compared to TETA, for stably chelating ^{64}Cu *in vivo*,[28] CB-TE2A was conjugated to Y3-TATE and directly compared to the ^{64}Cu-TETA-Y3-TATE conjugate.[69] ^{64}Cu-CB-TE2A-Y3-TATE was radiolabeled in high radiochemical purity with specific activities of 1.3–5.1 mCi/μg of peptide at 95°C and pH 8.0.[70] Biodistribution studies, using AR42J tumors implanted in male Lewis rats, revealed that this complex had higher uptake in somatostatin-positive tissues, compared to the TETA conjugate. Accumulation of ^{64}Cu-CB-TE2A-Y3-TATE was lower at all time points, in blood and liver, and less accumulation was observed in the kidney at earlier time points, when compared to ^{64}Cu-TETA-Y3-TATE. For example, the tumor-to-blood (T/B) ratio at 4 hours for ^{64}Cu-CB-TE2A-Y3-TATE was 156 ± 55; for ^{64}Cu-TETA-Y3-TATE, the T/B ratio was 8.2 ± 1.6 ($p < 0.001$). These data suggest that the ^{64}Cu-CB-TE2A-Y3-TATE is more resistant to transchelation than the TETA analog.

The majority of somatostatin analogs that have been evaluated for PET and SPECT imaging are somatostatin agonists, and as such, they are internalized into cells *via* receptor-mediated endocytosis and mimic the behavior of somatostatin itself. The belief has been that greater cellular internalization of a radiolabeled somatostatin analog *in vitro* is a predictor of improved tumor uptake *in vivo*. This has been demonstrated by the group at Rotterdam for ^{111}In-labeled somatostatin analogs[71,72] as well as by our group.[24,69] In 2006, Ginj et al. showed that an ^{111}In-labeled somatostatin receptor type 2 (SSTr2) antagonist, sst2-ANT, had improved uptake, compared to ^{111}In-DTPA-Y3-TATE,[73] in mice bearing SSTr2-transfected HEK-cell tumors. The researchers showed that sst2-ANT was not internalized in the HEK cells and demonstrated classical antagonist behavior. ^{64}Cu-CB-TE2A-sst2-ANT was compared with ^{64}Cu-CB-TE2A-Y3-TATE in AR42J tumor-bearing rats.[74] ^{64}Cu-CB-TE2A-sst2-ANT showed low levels of internalization in AR42J cells and similar uptake to ^{64}Cu-CB-TE2A-Y3-TATE *in vivo* at early time points. An interesting characteristic of the SSTr2 antagonist is that it appears to bind to ~15-fold higher number of receptors than the agonist (23,000 versus 1551 fmol/mg protein), but with ~17-fold decreased affinity (26 vs 1.5 nM). However, ^{64}Cu-CB-TE2A-sst2-ANT showed longer retention in the AR42J tumor, resulting in improved T/B (72) and T/M (93) ratios at 24 hour postinjection, compared to ^{64}Cu-CB-TE2A-Y3-TATE (T/B, 20; T/M, 45).[74]

Copper-64-Labeled Integrin-Targeting Peptides

Integrins are transmembrane proteins that regulate cell-cell and cell-matrix interactions. They are dimers that consist of two noncovalently bound subunits (α and β) that have an extra-

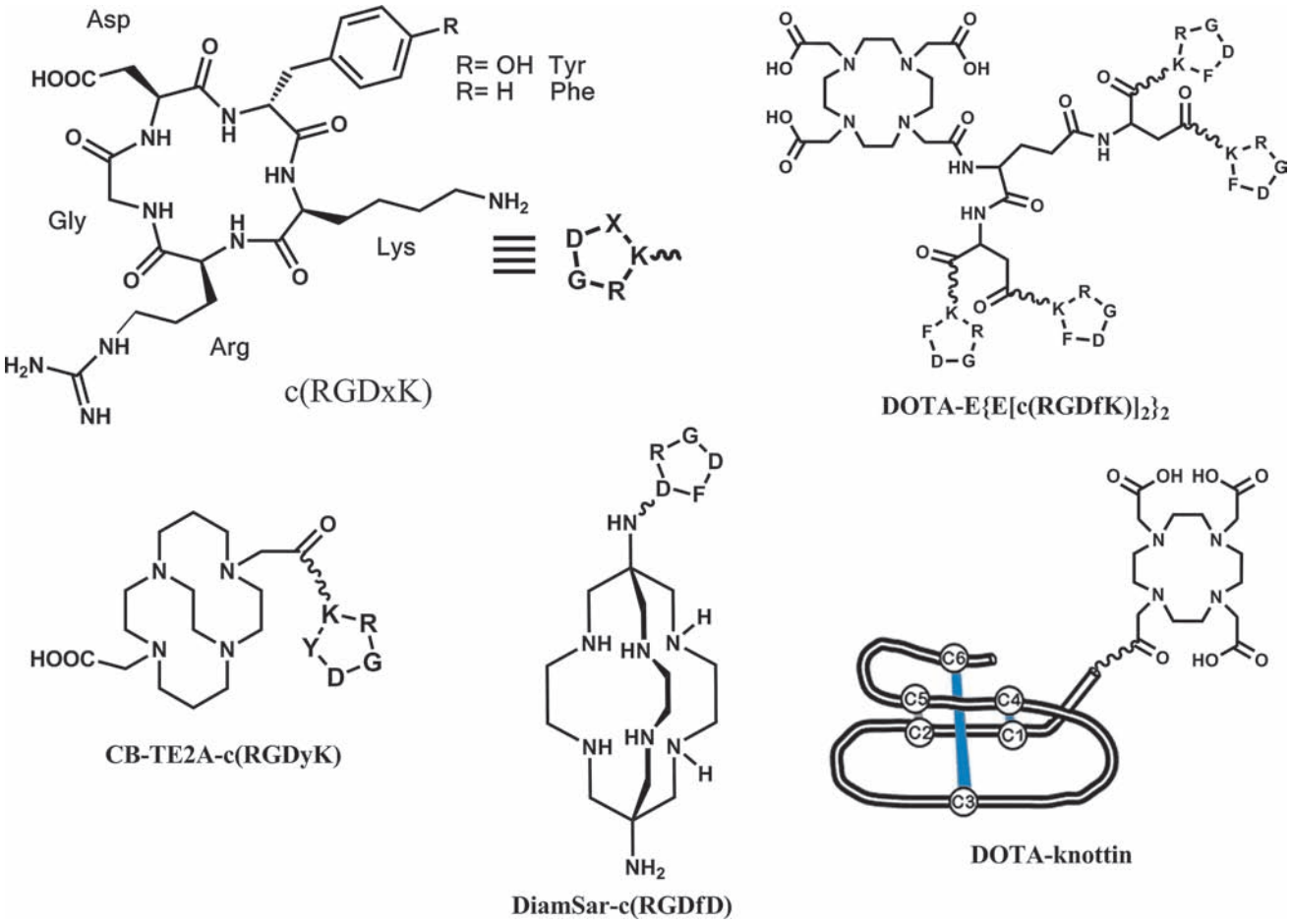

FIG. 4. Structures of c(RGDxK) peptides and proteins used in the imaging of $\alpha_v\beta_3$ expression in tumor angiogenesis and osteoclasts. x, D-Tyr or D-Phe.

cellular domain arranged in a characteristic way that imparts different adhesion properties to the cell.[75] Integrin proteins have been found to play important roles in angiogenesis and tumor metastasis. So far, 24 different integrins have been identified, constituted by combinations of 18-α and 8-β subunits. Alpha v beta 3 ($\alpha_v\beta_3$) is one of the most widely studied integrins, since it is upregulated in endothelial cells involved in active angiogenesis but not in quiescent endothelial cells,[76] making it an ideal biomarker for angiogenesis and tumor imaging.[77] Tumors where $\alpha_v\beta_3$ are found to be highly expressed include glioblastomas, breast and prostate tumors, malignant melanomas, and ovarian carcinomas.[78–81] The $\alpha_v\beta_3$ integrin binds to extracellular proteins through a specific binding pocket that recognizes the three-amimo-acid sequence, arginine-glycine-aspartic acid (Arg-Gly-Asp or RGD).[82,83] This discovery has led to the design of many RGD-based imaging agents,[77,84,85] and several investigations involving the ^{64}Cu radiolabeled complexes have been reported (Figure 4).

Chen et al. conjugated 1,4,7,10-tetraazacyclododecane-1,4,7,10-tetraacetic acid (DOTA) to c(RGDyK) and labeled it with ^{64}Cu for breast-cancer imaging studies but found only moderate uptake in U87MG human glioma tumors [1.44 ± 0.09 percent injected dose per gram [%ID/g] at 4 hour postinjection] with relatively high liver and kidney retention (2.84 ± 0.17 and 1.98 ± 0.06 %ID/g at 4 hour postinjection, respectively).[86] In order to improve tumor uptake and *in vivo* kinetics, they substituted the monomeric RGD derivative for dimeric compounds (E[c(RGDyK)$_2$ and E[c(RGDfK)$_2$) and observed improved tumor targeting. However, kidney uptake remained too high for the compounds to be considered for further clinical studies.[16] In an attempt to modulate kidney retention, polyethylene glycol (PEG) groups were added to the monomeric RGD peptide derivative, and it was observed that ^{64}Cu-DOTA-c(RGDyK)-PEG had very similar uptake in brain tumors, compared to ^{64}Cu-DOTA-c(RGDyK), but a much lower liver uptake and a faster clearance from blood and kidneys.[15] By using tetrameric[87] and octameric[88] RGD derivatives, binding affinity and tumor uptake in glioblastoma cells improved; however, liver and kidney uptake were also increased. Shi et al. examined the effects of linkages (Gly-Gly-Gly and PEG$_4$) between cyclic RGD dimers for agents labeled with ^{64}Cu by using the DOTA chelator.[89] This group showed that these linkages improved the tumor uptake, compared to simple RGD dimers, potentially due to having the appropriate distance between the two RGD peptides that allows binding to two different receptors simultaneously. This strategy can be applied to other receptors as well using molecular modeling to determine the distances between receptors on tumor cells.

In a recent patent, Kimura et al. reported on the conjugation of DOTA to a library of many "miniproteins" derived from knottin peptides whose 25–40-amino-acid sequences have been enriched by an RGD loop.[90] After screening for initial

integrin-binding ability, some of the chelators were labeled with ^{64}Cu. Biodistribution and micro-PET imaging studies showed good specific uptake in U87MG tumors (glioblastoma). However, kidney uptake was consistently higher than tumor uptake over a 25-hour period.[90]

Sprague et al. conjugated c(RGDyK) to a different chelator, CB-TE2A, and found that the corresponding ^{64}Cu complex was taken up specifically by osteoclasts,[91] which are upregulated in osteolytic lesions and bone metastases.[92] These investigations open the possibility of other applications for imaging $\alpha_v\beta_3$ in diseases, such as osteoarthritis or osteoporosis, as well as imaging osteolytic bone metastases.

Wei et al. compared two RGD peptides labeled with two highly stable chelating systems, CB-TE2A-c(RGDyK) and diamsar-c(RGDfD), in M21 and M21L human melanoma tumor-bearing mice.[93] This study showed that although both chelator-peptide conjugates had similar binding affinity for isolated $\alpha_v\beta_3$, the tumor targeting *in vivo* was better for ^{64}Cu-CB-TE2A-c(RGDyK) than the diamsar analog. There was also improved blood and liver clearance for ^{64}Cu-CB-TE2A-c(RGDyK). Some of these differences could be due to the differences in the peptides used, as well as the fact that diamsar had a very short linkage between the aspartic acid in the 5-position and the chelator.

^{64}Cu-Labeled Antibodies for Tumor Targeting

Targeting epidermal growth factor receptor 1

The epidermal growth factor (EGF) family of membrane receptors (EGFR) is one of the most relevant targets in the tyrosine kinase family. EGFR expression is increased in many human tumors such as breast cancer, squamous-cell carcinoma of the head and neck, and prostate cancer.[94] Activation of EGFR contributes to several tumorigenic mechanisms, and in many tumors, EGFR expression may act as a prognostic indicator, predicting patient survival and/or more of the presence of diseases in advanced stages.[94] At present, monoclonal antibodies (mAbs), which block the binding of EGF to the extracellular ligand-binding domain of the receptor, have shown promise from a therapeutic standpoint. Cetuximab (C225; Erbitux,® Bristol-Myers Squibb, New York, NY) was the first mAb targeted against the EGFR approved by the U.S. Food and Drug Administration (FDA) for the treatment of patients with EGFR-expressing, metastatic colorectal carcinoma. Cetuximab binds competitively to the extracellular domain of EGFR with an affinity comparable to the natural ligand ($K_D = 1.0$ nM), inhibiting the binding of the activating ligand to the receptor.[95,96]

Cai et al. reported the evaluation of ^{64}Cu-DOTA-cetuximab in several tumor-bearing mouse models.[97] Using Western blot analysis, a positive correlation was shown to exist between the expression of EGFR and uptake of ^{64}Cu-DOTA-cetuximab in several different EGFR-expressing tumor-bearing mouse models. At Washington University, St. Louis, MO, ^{64}Cu-DOTA-cetuximab was synthesized for the small-animal PET imaging of EGFR expression in A431 tumor-bearing mice.[98] Highly EGFR-expressing A431 and low-EGFR-expressing MDA-MB-435 cells were compared. An equilibrium dissociation constant (K_D) of 0.28 nM was obtained with the A431 cells, and the K_D and B_{max} (maximum receptor density) were in agreement with the reported literature values of unlabeled cetuximab with A431 cells.[98] *In vivo* evaluation of ^{64}Cu-DOTA-cetuximab was performed in A431 and MDA-MB-435 tumor-bearing mice. Both biodistribution and micro-PET data showed a higher uptake in the EGFR-positive A431 (Figure 5) tumor than in the EGFR-negative MDA-MB-435 tumor. Metabolism experiments were also performed to determine the extent of ^{64}Cu transchelation to blood, liver, and tumor proteins in A431 tumor-bearing mice. The results showed minimal metabolism of ^{64}Cu-DOTA-cetuximab in the blood out to 24 hours postinjection. Liver metabolism studies, using size-exclusion chromatography, demonstrated that transchelation of ^{64}Cu to three proteins occurs; these were identified as SOD and metallothionein, while the third metabolite was believed to be a protein aggregate.

^{64}Cu-DOTA-cetuximab has also been evaluated for correlating EGFR densities on the surface of five different cervical cancer lines with the EGFR-messenger RNA (mRNA) expression. Based on the cellular data, micro-PET imaging was performed on tumor-bearing mice, using the highest expressing cervical cancer cell line, CaSki. For the *in vitro* analysis, five cervical cancer cell lines were selected after a screen of 23 human cervical cancer lines, based on their level of EGFR gene expression by gene-expression microarray analysis. The five cell lines had different ranges of EGFR expression with the following order: CaSki (high), ME-180 and DcTc2 4510 (both midrange), HeLa (low), and C-33A (negative). The cell-surface EGFR expression was evaluated by conducting saturation binding assays at 4°C, and the results paralleled the levels of EGFR expression determined by microarray analysis. *In vivo* biodistribution and small-animal PET studies with ^{64}Cu-DOTA-cetuximab in CaSki tumor-bearing nude mice showed relatively high tumor uptake at 24 hour after injection (13.2 %ID/g), with significant retention of radioactivity in blood and liver as well. Overall, this study demonstrated that ^{64}Cu-DOTA-cetuximab is a useful marker of EGFR-expression levels, as well as a potential PET agent for determining patient-specific therapies and therapeutic monitoring.

Other ^{64}Cu-labeled mAbs for tumor targeting

The SarAr chelator was attached to the anti-GD2 mAb, 14.G2a, and its chimeric analog, ch14.18, that target disialogangliosides overexpressed on neuroblastoma and melanoma.[99] Biodistribution studies in athymic nude mice bearing subcutaneous (s.c.) neuroblastoma (IMR-6, NMB-7) and melanoma (M21) xenografts showed that 15%–20% of the ID/G accumulated in the tumor at 24 hours after injection, and only 5%–10% of the ID accumulated in the liver, a lower value than typically seen with other chelators. Uptake by a GD2-negative tumor xenograft was significantly lower (<5 %ID/G). This study demonstrates the utility of the highly stable SarAr chelation system, which enables the formation of stable ^{64}Cu complexes attached to mAbs by using mild radiolabeling conditions.

Copper-64-Labeled Nanoparticles

Nanotechnology is an applied science that creates and studies molecules or aggregates that have an overall size in the 1–1000-nm range (<1 μm). In the last few years, nanodevices and -particles have been used in biomedical studies

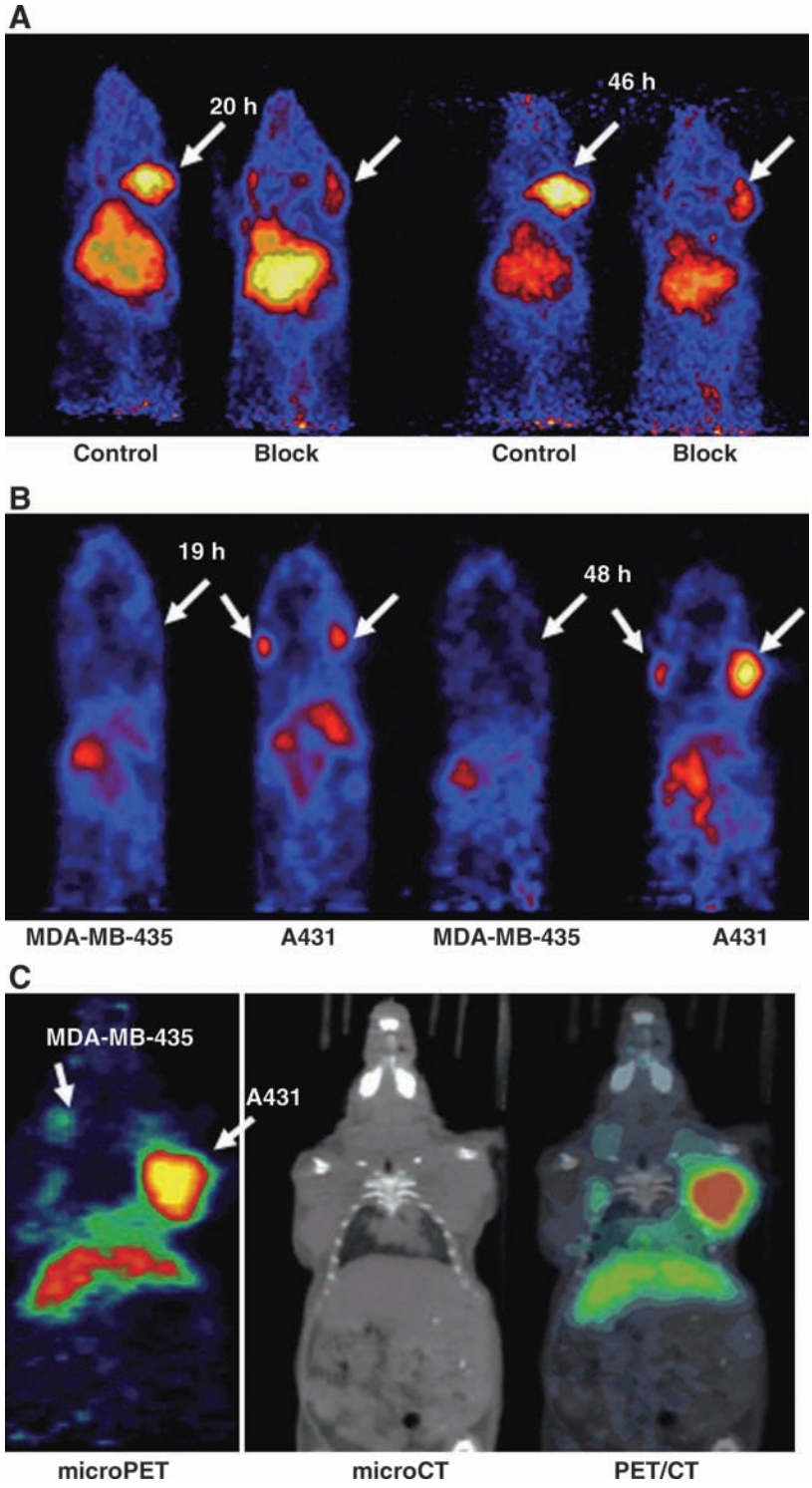

FIG. 5. (**A**) Projection micro-PET (positron emission tomography) images of A431 tumor-bearing nude mice after 20 and 46 hours postadministration of ^{64}Cu-DOTA-cetuximab, with and without an injected blocking dose 20 hours prior to the imaging dose (5.6 MBq, 6 g, left; 5.6 MBq, 1 mg of cetuximab, right). (**B**) Coronal micro-PET images of ^{64}Cu-DOTA-cetuximab in A431 [epidermal growth factor receptor (EGFR)-positive] and MDA-MB-435 (EGFR-negative) tumor-bearing mice after 19 and 48 hours postadministration of ^{64}Cu-DOTA-cetuximab. (**C**) micro-PET/computed tomography coregistration images of ^{64}Cu-DOTA-cetuximab in a mouse bearing both A431 and MDA-MB-435 tumors (arrow) at 24 hours postinjection. Reprinted by permission of the Mary Ann Liebert, Inc., publishers from reference 98.

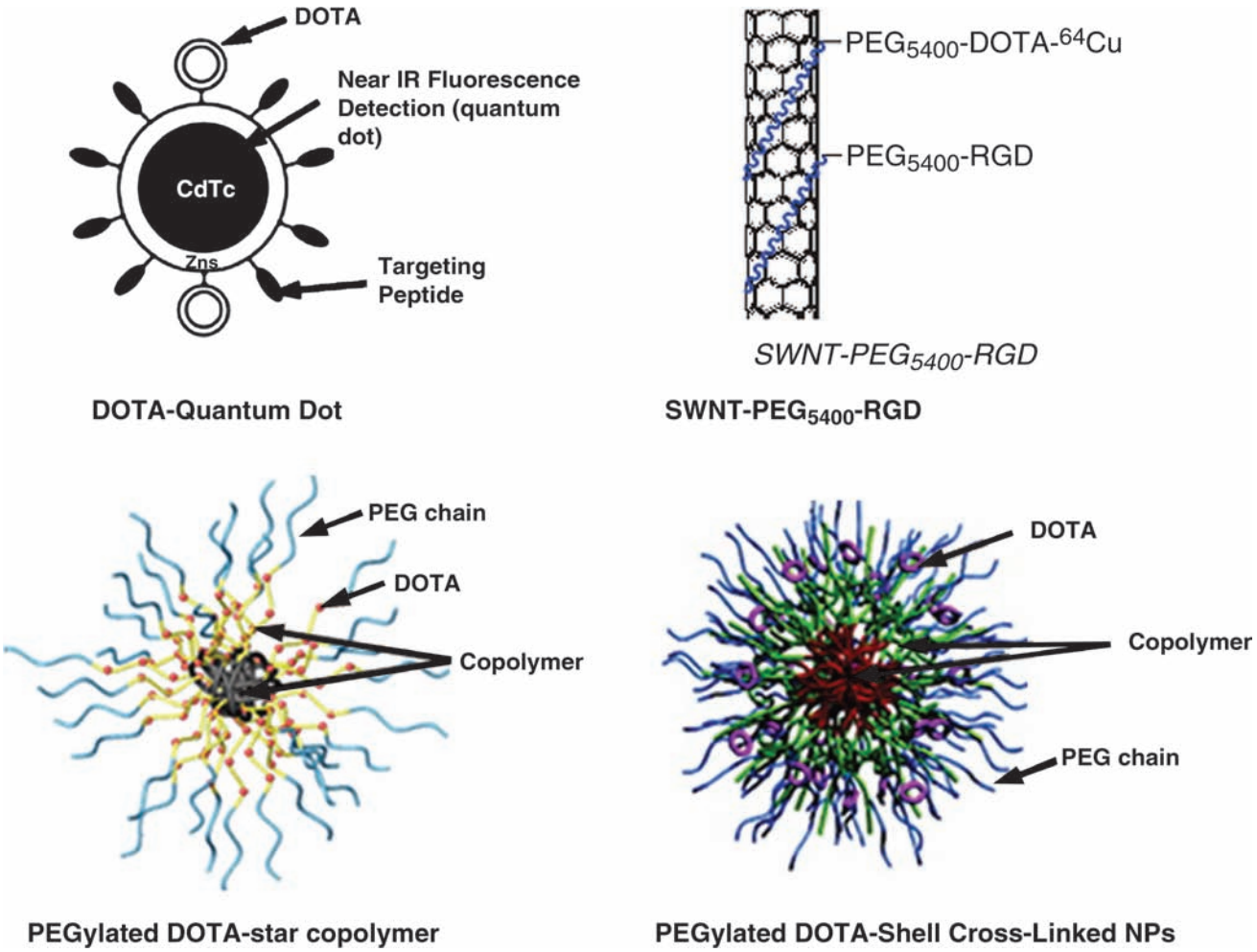

FIG. 6. Structures of nanoparticles used in imaging include DOTA-conjugated quantum dots,[123] DOTA- and RGD peptide-conjugated single-walled carbon nanotube nanoparticles,[115] PEGylated DOTA star copolymers,[120] and PEGylated DOTA-shell cross-lined (SCK) nanoparticles.[104]

investigating new and improved diagnosis and therapy agents. Oncology is one of the disciplines that has benefited the most from nanotechnology. Several nanoparticles are used in diagnostic assays for cancer, as contrast agents for MRI, as drug-delivery agents, as tumor visualization agents during surgery, and as therapeutic agents.[100,101] Several types of nanoparticle platforms have been evaluated for imaging applications, including iron-oxide nanoparticles,[88,102–104] gold nanoparticles,[105–108] liposomes,[109,110] emulsions,[111,112] dendrimers,[113,114] and nanotubes (see Figure 6 for some examples).[115–117] Nanoparticles conjugated with bifunctional chelators and targeting ligands are particularly useful for PET imaging purposes because their higher surface area per volume allows a higher number of targeting residues and radionuclides per particle, which, in turn, translates into higher affinity and higher specific activity, respectively.[118]

Studies have been performed to determine the pharmacokinetics of nontargeted nanostructures labeled with ^{64}Cu by using the DOTA chelator. Pressly et al. prepared well-defined amphiphilic copolymers with a predetermined number of reactive functionalities, with PEG chains of variable length and low polydispersity.[119] Upon collapsing in water, these polymers formed three-dimensional, three-layered nanoparticles with a hydrophobic inner core surrounded by a hydrophilic shell where the functional groups are located and, finally, a PEG outer shell. The thickness of each layer, the number of reactive sites, and the dimension of the particle are determined by the composition of the initial linear polymer. When DOTA molecules were conjugated to these nanoparticles, ^{64}Cu labeling was achieved and biodistribution studies were conducted. Not surprisingly, particles with longer PEG-chain length had longer circulation in blood and lower liver uptake.[119,120]

Sun et al. synthesized shell-cross-linked nanoparticles (SCKs) by cross-linking to different degree micelles formed by amphiphilic block copolymers. When TETA was incorporated onto the final SCKs, the yield was low and the labeling efficiency was unsatisfactory.[121] This problem was solved by preincorporating the copper chelator (DOTA in this case) into the copolymer before the nanoparticles were formed.[104] Tuning of the pharmacokinetics of these particles was performed by introducing different numbers and different lengths of PEG chains.[104] The extent of cross-linking and the dimensions of the linker between nanoparticle and

copper chelator were found to have a dramatic impact on the specific activity of the radiolabeled particle.[122]

The majority of targeted nanoparticles that have been evaluated have been conjugated with RGD peptide for the targeting of $\alpha_v\beta_3$ integrin. Cai et al. conjugated c(RGDyK) and DOTA to quantum dots (QD), obtaining a 20-nm nanoparticle having about 28 DOTA and 90 RGD residues on its surface.[123] They observed selective targeting of the vasculature of $\alpha_v\beta_3$-positive tumors, such as U87MG human glioblastoma, with minimal extravasation, which would be necessary for high tumor uptake. This led to a lower than expected tumor uptake, with most of the ^{64}Cu-DOTA-QD-RGD being taken up by the liver, spleen, and bone marrow. The researchers concluded that smaller particles would probably have improved tumor-targeting properties due to easier extravasation and lower reticuloendothelial system uptake.[123] Lee et al. reported 5-nm iron-oxide nanoparticles coated with polyaspartic acid functionalized with an estimated 35 RGD peptides and 30 DOTA macrocycles per particle.[124] PET studies gave high contrast images of the tumor; however, liver uptake was still high. This behavior may be explained by the fact that while the core diameter of the particles was 5 nm, their hydrodynamic size was much larger (45 nm), so the same problems observed with the QD nanoparticles persisted.[124]

One of the most successful examples of tumor targeting with ^{64}Cu-labeled RGD-conjugated nanoparticles involves the use of single-walled carbon nanotubes (SWNTs).[115] Here, a comparison of SWNT that contained different sizes of PEG was evaluated in U87MG human glioblastoma tumor-bearing mice. The best conjugates were ^{64}Cu-SWNT-PEG$_{5400}$-RGD, which showed the lowest liver and highest tumor accumulation that was improved over nontargeted SWNT.

Conclusions

^{64}Cu-based radiopharmaceuticals are being explored as agents for the delineation of disease in humans. By exploitation of the chemistry of Cu(II) and the decay characteristics of ^{64}Cu, agents based on small molecules, peptides, and larger biomolecules, such as antibodies and nanoparticles, are in development for clinical translation. A diverse array of highly specific molecular ^{64}Cu-radiopharmaceutical imaging probes will inevitably lead to improved patient-specific treatments.

Acknowledgments

The authors gratefully acknowledge National Institutes of Health (NIH; Bethesda, MD) grants R01 CA64475, R01 CA093375, and U01 HL080729-01 for funding in research in the area of this review article.

Disclosure Statement

No competing financial interests exist.

References

1. Szelecsenyi F, Blessing G, Qaim SM. Excitation function of proton-induced nuclear reactions on enriched ^{61}Ni and ^{64}Ni: Possibility of production of no-carrier-added ^{61}Cu and ^{64}Cu at a small cyclotron. Appl Radiat Isot 1993;44:575.
2. McCarthy DW, Shefer RE, Klinkowstein RE, et al. Efficient production of high-specific-activity ^{64}Cu using a biomedical cyclotron. Nucl Med Biol 1997;24:35.
3. Zweit J, Smith AM, Downey S, Sharma HL. Excitation functions for deuteron induced reactions in natural nickel: Production of no-carrier-added ^{64}Cu from enriched ^{64}Ni targets for positron emission tomography. Appl Radiat Isot 1991;42:193.
4. Obata A, Kasamatsu S, McCarthy DW, et al. Production of therapeutic quantities of ^{64}Cu using a 12-MeV cyclotron. Nucl Med Biol 2003;30:535.
5. McCarthy DW, Bass LA, Cutler PD, et al. High-purity production and potential applications of copper-60 and copper-61. Nucl Med Biol 1999;26:351.
6. Zeissler SK, Pavan RA, Orzechowski J, et al. Production of ^{64}Cu on the Sherbrooke TR-PET cyclotron. J Radioanal Nucl Chem 2003;257:175.
7. Avila-Rodriguez MA, Nye JA, Nickles RJ. Simultaneous production of high specific activity ^{64}Cu and ^{61}Co with 11.4-MeV protons on enriched ^{64}Ni nuclei. Appl Radiat Isot 2007;65:1115.
8. Szajek LP, Meyer W, Plascjak P, Eckleman WC. Semi-remote production of [^{64}Cu]$CuCl_2$ and preparation of high-specific-activity [^{64}Cu]Cu-ATSM for PET studies. Radiochim Acta 2005;93:239.
9. Lewis JS, Welch MJ, Tang L. Workshop on the production, application, and clinical translation of "non-standard" PET nuclides: A meeting report. Q J Nucl Med Mol Imaging 2008;52:101.
10. Linder MC. Biochemistry of Copper. New York: Plenum Press, 1991.
11. Linder MC, Hazegh-Azam M. Copper biochemistry and molecular biology. Am J Clin Nutr (Suppl) 1996;63:797s.
12. Frieden E. Perspectives on copper biochemistry. Clin Physiol Biochem 1986;4:11.
13. Wu Y, Zhang X, Xiong Z, et al. micro-PET imaging of glioma integrin $\alpha_v\beta_3$ expression using ^{64}Cu-labeled tetrameric RGD peptide. J Nucl Med 2005;46:1707.
14. McQuade P, Miao Y, Yoo J, et al. Imaging of melanoma using ^{64}Cu- and ^{86}Y-DOTA-ReCCMSH(Arg11), a cyclized peptide analogue of alpha-MSH. J Med Chem 2005;48:2985.
15. Chen X, Hou Y, Tohme M, et al. Pegylated Arg-Gly-Asp peptide: ^{64}Cu labeling and PET imaging of brain tumor alphavbeta3-integrin expression. J Nucl Med 2004;45:1776.
16. Chen X, Liu S, Hou Y, et al. micro-PET imaging of breast cancer alphav-integrin expression with ^{64}Cu-labeled dimeric RGD peptides. Mol Imaging Biol 2004;6:350.
17. Chen X, Sievers E, Hou Y, et al. Integrin alpha v beta 3–targeted imaging of lung cancer. Neoplasia 2005;7:271.
18. Li WP, Lewis JS, Kim J, et al. DOTA-D-Tyr(1)-octreotate: A somatostatin analogue for labeling with metal and halogen radionuclides for cancer imaging and therapy. Bioconjug Chem 2002;13:721.
19. Moi MK, Meares CF, McCall MJ, et al. Copper chelates as probes of biological systems: Stable copper complexes with a macrocyclic bifunctional chelating agent. Anal Biochem 1985;148:249.
20. Anderson CJ, Pajeau TS, Edwards WB, et al. *In vitro* and *in vivo* evaluation of copper-64-octreotide conjugates. J Nucl Med 1995;36:2315.
21. Anderson CJ, Jones LA, Bass LA, et al. Radiotherapy, toxicity and dosimetry of copper-64-TETA-octreotide in tumor-bearing rats. J Nucl Med 1998;39:1944.

22. Anderson CJ, Dehdashti F, Cutler PD, et al. ^{64}Cu-TETA-octreotide as a PET imaging agent for patients with neuroendocrine tumors. J Nucl Med 2001;42:213.
23. Lewis JS, Srinivasan A, Schmidt MA, Anderson CJ. *In vitro* and *in vivo* evaluation of ^{64}Cu-TETA-Tyr^3-octreotate. A new somatostatin analog with improved target tissue uptake. Nucl Med Biol 1999;26:267.
24. Lewis JS, Lewis MR, Srinivasan A, et al. Comparison of four ^{64}Cu-labeled somatostatin analogues *in vitro* and in a tumor-bearing rat model: Evaluation of new derivatives for positron emission tomography imaging and targeted radiotherapy. J Med Chem 1999;42:1341.
25. Lewis MR, Boswell CA, Laforest R, et al. Conjugation of monoclonal antibodies with TETA using activated esters: biological comparison of 64Cu-TETA-1A3 with ^{64}Cu-BAT-2IT-1A3. Cancer Biother Radiopharm 2001;16:483.
26. Philpott GW, Schwarz SW, Anderson CJ, et al. Radioimmuno-PET: Detection of colorectal carcinoma with positron-emitting copper-64-labeled monoclonal antibody. J Nucl Med 1995;36:1818.
27. Bass LA, Wang M, Welch MJ, Anderson CJ. *In vivo* transchelation of copper-64 from TETA-octreotide to superoxide dismutase in rat liver. Bioconjug Chem 2000;11:527.
28. Boswell CA, Sun X, Niu W, et al. Comparative *in vivo* stability of copper-64-labeled cross-bridged and conventional tetraazamacrocyclic complexes. J Med Chem 2004;47:1465.
29. Sargeson AM. The potential for the cage complexes in biology. Coord Chem Rev 1996;151:89.
30. Smith SV, Waters DJ, DiBartolo N. Separation of ^{64}Cu from ^{67}Ga waste products using anion exchange and low-acid aqueous/organic mixtures. Radiochimica Acta 1996;75:65.
31. Weisman GR, Rogers ME, Wong EH, et al. Cross-bridged cyclam. Protonation and Li^+ complexation in a diamond-lattice cleft. J Am Chem Soc 1990;112:8604.
32. Weisman GR, Wong EH, Hill DC, et al. Synthesis and transition-metal complexes of new cross-bridged tetraamine ligands. J Chem Soc Chem Commun 1996:947.
33. Hubin TJ, McCormick JM, Collinson SR, et al. Ultra rigid cross-bridged tetraazamacrocycles as ligands—the challenge and the solution. Chem Commun (Camb) 1998: 1675.
34. Hubin TJ, Alcock NW, Busch DH. The square-pyramidal PdII complex of a cross-bridged tetraazamacrocycle. Acta Crystallogr 1999;C55:1404.
35. Hubin TJ, McCormick JM, Alcock NW, et al. Crystallographic characterization of stepwise changes in ligand conformation as their internal topology changes and two novel cross-bridged tetraazamacrocyclic copper(II) complexes. Inorg Chem 1999;38:4435.
36. Hubin TJ, Alcock NW, Morton MD, et al. Synthesis, structure, and stability in acid of copper(II) and zinc(II) complexes of cross-bridged tetraazamacrocycles. Inorganica Chimica Acta 2003;348:33.
37. Niu W, Wong EH, Weisman GR, et al. Copper(II) and zinc(II) complexes of amide pendant-armed cross-bridged tetraamine ligands. Polyhedron 2004;23:1019.
38. Hubin TJ, Alcock NW, Busch DH. Copper(I) and copper(II) complexes of an ethylene cross-bridged cyclam. Acta Crystallogr 2000;C56:37.
39. Wong EH, Weisman GR, Hill DC, et al. Synthesis and characterization of cross-bridged cyclams and pendant-armed derivatives and structural studies of their copper(II) complexes. J Am Chem Soc 2000;122:10561.
40. Sun X, Wuest M, Weisman GR, et al. Radiolabeling and *in vivo* behavior of copper-64-labeled cross-bridged cyclam ligands. J Med Chem 2002;45:469.
41. Woodin KS, Heroux KJ, Boswell CA, et al. Kinetic inertness and electrochemical behavior of Cu(II) tetraazamacrocyclic complexes: Possible implications for *in vivo* stability. Eur J Inorg Chem 2005;23:4829.
42. Heroux KJ, Woodin KS, Tranchemontagne DJ, et al. The long and short of it: The influence of N-carboxyethyl versus N-carboxymethyl pendant arms on *in vitro* and *in vivo* behavior of copper complexes of cross-bridged tetraamine macrocycles. Dalton Trans 2007:2150.
43. Anderson CJ, Wadas TJ, Wong EH, et al. Cross-bridged macrocyclic chelators for stable complexation of copper radionuclides for PET imaging. Q J Nucl Med Mol Imaging 2008;52:185.
44. Kotek J, Lubal P, Hermann P, et al. High thermodynamic stability and extraordinary kinetic inertness of copper(II) complexes with 1,4,8,11-tetraazacyclotetradecane-1,8-bis (methylphosphonic acid): Example of a rare isomerism between kinetically inert penta- and hexacoordinated copper(II) complexes. Chem Eur J 2003;9:233.
45. Lukes I, Kotek J, Vojtisek P, et al. Complexes of tetraazacycles bearing methylphosphinic/phosphonic acid pendant arms with copper(II), zinc(II), and lanthanides(III). A comparison with their acetic acid analogues. Coord Chem Rev 2001;216:287.
46. Sun X, Wuest M, Kovacs Z, et al. *In vivo* behavior of copper-64-labeled methanephosphonate tetraazamacrocyclic ligands. J Biol Inorg Chem 2003;8:217.
47. Ferdani R, Stigers DJ, Sherman CD, et al. New phosphonic acid derivatives of cross-bridged cyclam as ^{64}Cu chelators. J Radiolab Comp Radiopharm 2009;52(suppl1):56.
48. Boswell CA, Regino CA, Baidoo KE, et al. A novel side-bridged hybrid phosphonate/acetate pendant cyclam: Synthesis, characterization, and ^{64}Cu small animal PET imaging. Bioorg Med Chem 2009;17:548.
49. Brown JM. The hypoxic cell: A target for selective cancer therapy—eighteenth Bruce F. Cain Memorial Award lecture. Cancer Res 1999;59:5863.
50. Tatum JL, Kelloff GJ, Gillies RJ, et al. Hypoxia: Importance in tumor biology, noninvasive measurement by imaging, and value of its measurement in the management of cancer therapy. Int J Radiat Biol 2006;82:699.
51. Hockel M, Schlenger K, Aral B, et al. Association between tumor hypoxia and malignant progression in advanced cancer of the uterine cervix. Cancer Res 1996;56:4509.
52. Fujibayashi Y, Taniuchi H, Yonekura Y, et al. Copper-62-ATSM: A new hypoxia imaging agent with high membrane permeability and low redox potential. J Nucl Med 1997; 38:1155.
53. Fujibayashi Y, Cutler CS, Anderson CJ, et al. Comparative imaging studies of ^{64}Cu-ATSM a hypoxia imaging agent and C-11-acetate in an acute myocardial infarction model: *Ex vivo* imaging in rats. Nucl Med Biol 1999;26:117.
54. Dearling JLJ, Lewis JS, Welch MJ, et al. Redox-active complexes for imaging hypoxic tissues: Structure-activity relationships in copper(II)bis(thiosemicarbazone) complexes. Chem Commun 1998;22:2531.
55. Dearling JL, Lewis JS, Mullen GE, et al. Copper bis(thiosemicarbazone) complexes as hypoxia imaging agents: Structure-activity relationships. J Biol Inorg Chem 2002; 7:249.

56. Lewis J, Laforest R, Buettner T, et al. Copper-64-diacetyl-bis(N4-methylthiosemicarbazone): An agent for radiotherapy. Proc Natl Acad Sci U S A 2001;98:1206.
57. Lewis JS, McCarthy DW, McCarthy TJ, et al. Evaluation of ^{64}Cu-ATSM *in vitro* and *in vivo* in a hypoxic tumor model. J Nucl Med 1999;40:177.
58. Holland JP, Barnard PJ, Collison D, et al. Spectroelectrochemical and computational studies on the mechanism of hypoxia selectivity of copper radiopharmaceuticals. Chemistry 2008;14:5890.
59. Dence CS, Ponde DE, Welch MJ, et al. Autoradiographic and small-animal PET comparisons between (18)F-FMISO, (18)F-FDG, (18)F-FLT, and the hypoxic selective (64)Cu-ATSM in a rodent model of cancer. Nucl Med Biol 2008; 35:713.
60. Takahashi N, Fujibayashi Y, Yonekura Y, et al. Evaluation of ^{62}Cu-labeled diacetyl-bis(N4-methylthiosemicarbazone) as a hypoxic tissue tracer in patients with lung cancer. Ann Nucl Med 2000;14:323.
61. Dehdashti F, Mintun MA, Lewis JS, et al. *In vivo* assessment of tumor hypoxia in lung cancer with ^{60}Cu-ATSM. Eur J Nucl Med Mol Imaging 2003;30:844.
62. Dehdashti F, Grigsby PW, Mintun MA, et al. Assessing tumor hypoxia in cervical cancer by positron emission tomography with ^{60}Cu-ATSM: Relationship to therapeutic response—a preliminary report. Int J Radiat Oncol Biol Phys 2003;55:1233.
63. Laforest R, Dehdashti F, Lewis JS, et al. Dosimetry of 60/61/62/64Cu-ATSM: A hypoxia imaging agent for PET. Eur J Nucl Med Mol Imaging 2005;32:764.
64. Lewis JS, Laforest R, Dehdashti F, et al. An imaging comparison of ^{64}Cu-ATSM and ^{60}Cu-ATSM in cancer of the uterine cervix. J Nucl Med 2008;49:1177.
65. Dehdashti F, Grigsby PW, Lewis JS, et al. Assessing tumor hypoxia in cervical cancer by PET with ^{60}Cu-labeled diacetyl-bis(N4-methylthiosemicarbazone). J Nucl Med 2008; 49:201.
66. Bauer W, Briner U, Doepfner W, et al. SMS 201-995: A very potent and selective octapeptide analogue of somatostatin with prolonged action. Life Sci 1982;31:1133.
67. Krenning EP, Bakker WH, Kooij PP, et al. Somatostatin receptor scintigraphy with indium-111-DTPA-D-Phe-1-octreotide in man: Metabolism, dosimetry, and comparison with iodine-123-Tyr-3-octreotide. J Nucl Med 1992; 33:652.
68. de Jong M, Breeman WA, Bakker WH, et al. Comparison of (111)In-labeled somatostatin analogues for tumor scintigraphy and radionuclide therapy. Cancer Res 1998;58:437.
69. Sprague JE, Peng Y, Sun X, et al. Preparation and biological evaluation of copper-64-labeled Tyr^3-octreotate using a cross-bridged macrocyclic chelator. Clin Cancer Res 2004; 10:8674.
70. Wadas TJ, Anderson CJ. Radiolabeling of TETA- and CB-TE2A-conjugated peptides with copper-64. Nat Protoc 2006;1:3062.
71. de Jong M, Bakker WH, Krenning EP, et al. Yttrium-90 and indium-111 labelling, receptor binding, and biodistribution of [DOTA^0,D-Phe^1,Tyr^3]octreotide, a promising somatostatin analogue for radionuclide therapy. Eur J Nucl Med 1997;24:368.
72. de Jong M, Bernard BF, de Bruin E, et al. Internalization of radiolabelled [DTPA^0]octreotide and [DOTA^0, Tyr^3] octreotide: Peptides for somatostatin receptor-targeted scintigraphy and radionuclide therapy. Nuc Med Commun 1998;19:283.
73. Ginj M, Zhang H, Waser B, et al. Radiolabeled somatostatin receptor antagonists are preferable to agonists for *in vivo* peptide receptor targeting of tumors. Proc Natl Acad Sci U S A 2006;103:16436.
74. Wadas TJ, Eiblmaier M, Zheleznyak A, et al. Preparation and biological evaluation of ^{64}Cu-CB-TE2A-sst2-ANT, a somatostatin antagonist for PET imaging of somatostatin receptor-positive tumors. J Nucl Med 2008;49:1819.
75. Hynes RO. Integrins: Versatility, modulation, and signaling in cell adhesion. Cell 1992;69:11.
76. Hood JD, Cheresh DA. Role of integrins in cell invasion and migration. Nat Rev Cancer 2002;2:91.
77. Beer AJ, Schwaiger M. Imaging of integrin alpha v beta 3 expression. Cancer Metast Rev 2008;27:631.
78. Albelda SM, Mette SA, Elder DE, et al. Integrin distribution in malignant melanoma: Association of the beta 3 subunit with tumor progression. Cancer Res 1990;50:6757.
79. Bello L, Francolini M, Marthyn P, et al. Alpha(v)beta3 and alpha(v)beta5 integrin expression in glioma periphery. Neurosurgery 2001;49:380.
80. Brooks PC, Stromblad S, Klemke R, et al. Antiintegrin alpha v beta 3 blocks human breast cancer growth and angiogenesis in human skin. J Clin Invest 1995;96:1815.
81. Jin H, Varner J. Integrins: Roles in cancer development and as treatment targets. B J Cancer 2004;90:561.
82. Horton MA. The alpha v beta 3 integrin "vitronectin receptor." Int J Biochem Cell Biol 1997;29:721.
83. Xiong J-P, Stehle T, Zhang R, et al. Crystal structure of the extracellular segment of integrin alpha vbeta 3 in complex with an Arg-Gly-Asp Ligand. Science 2002;296:151.
84. Janssen ML, Oyen WJ, Dijkgraaf I, et al. Tumor targeting with radiolabeled alpha(v)beta(3) integrin binding peptides in a nude mouse model. Cancer Res 2002;62:6146.
85. van Hagen PM, Breeman WA, Bernard HF, et al. Evaluation of a radiolabelled cyclic DTPA-RGD analogue for tumour imaging and radionuclide therapy. Int J Cancer 2000;90:186.
86. Chen X, Park R, Tohme M, et al. micro-PET and autoradiographic imaging of breast cancer alpha-v-integrin expression using ^{18}F- and ^{64}Cu-labeled RGD peptide. Bioconjug Chem 2004;15:41.
87. Wu Y, Zhang X, Xiong Z, et al. micro-PET imaging of glioma integrin {alpha}v{beta}3 expression using (64)Cu-labeled tetrameric RGD peptide. J Nucl Med 2005;46:1707.
88. Li ZB, Cai W, Cao Q, et al. (64)Cu-labeled tetrameric and octameric RGD peptides for small-animal PET of tumor alpha(v)beta(3) integrin expression. J Nucl Med 2007;48: 1162.
89. Shi J, Kim YS, Zhai S, et al. Improving tumor uptake and pharmacokinetics of (64)Cu-labeled cyclic RGD peptide dimers with Gly(3) and PEG(4) linkers. Bioconjug Chem 2009;20:750.
90. Kimura RH, Cheng Z, Gambhir SS, et al. Engineered knottin peptides: A new class of agents for imaging integrin expression in living subjects. Cancer Res 2009;69:2435.
91. Sprague JE, Kitaura H, Zou W, et al. Noninvasive imaging of osteoclasts in parathyroid hormone-induced osteolysis using a ^{64}Cu-labeled RGD peptide. J Nucl Med 2007;48:311.
92. Nakamura I, Duong le T, Rodan SB, Rodan GA. Involvement of alpha(v)beta3 integrins in osteoclast function. J Bone Miner Metab 2007;25:337.

93. Wei L, Ye Y, Wadas TJ, et al. (64)Cu-Labeled CB-TE2A and diamsar-conjugated RGD peptide analogs for targeting angiogenesis: comparison of their biological activity. Nucl Med Biol 2009;36:277.
94. Laskin JJ, Sandler AB. Epidermal growth factor receptors: A promising target in solid tumors. Cancer Treat Rev 2004;30:1.
95. Fan Z, Masui H, Altas I, Mendelsohn J. Blockage of epidermal growth factor receptor function by bivalent and monovalent fragments of C225 antiepidermal growth factor receptor monoclonal antiobodies. Cancer Res 1993;53:4322.
96. Mendelsohn J. Epidermal growth factor receptor inhibition by a monocolonal antobody as anticancer therapy. Clin Cancer Res 1997;3:2703.
97. Cai W, Chen K, He L, et al. Quantitative PET of EGFR expression in xenograft-bearing mice using (64)Cu-labeled cetuximab, a chimeric anti-EGFR monoclonal antibody. Eur J Nucl Med Mol Imaging 2007;34:850.
98. Li WP, Meyer LA, Capretto DA, et al. Receptor-binding, biodistribution, and metabolism studies of ^{64}Cu-DOTA-cetuximab, a PET-imaging agent for epidermal growth-factor receptor-positive tumors. Cancer Biother Radiopharm 2008;23:158.
99. Xue C-B, Voss ME, Nelson DJ, et al. Design, synthesis, and structure-activity relationships of macrocyclic hydroxamic acids that inhibit tumor necrosis factor α relaease *in vitro* and *in vivo.* J Med Chem 2001;44:2636.
100. Banerjee HN, Verma M. Application of nanotechnology in cancer. Technol Cancer Res Treat 2008;7:149.
101. Jain KK. Recent advances in nanooncology. Technol Cancer Res Treat 2008;7:1.
102. Lanza GM, Winter P, Caruthers S, et al. Novel paramagnetic contrast agents for molecular imaging and targeted drug delivery. Curr Pharm Biotechnol 2004;5:495.
103. Sosnovik DE, Nahrendorf M, Weissleder R. Magnetic nanoparticles for MR imaging: Agents, techniques, and cardiovascular applications. Basic Res Cardiol 2008;103: 122.
104. Sun G, Hagooly A, Xu J, et al. Facile, efficient approach to accomplish tunable chemistries, and variable biodistributions for shell cross-linked nanoparticles. Biomacromolecules 2008;9:1997.
105. Hirsch LR, Gobin AM, Lowery AR, et al. Metal nanoshells. Ann Biomed Eng 2006;34:15.
106. Kogan MJ, Olmedo I, Hosta L, et al. Peptides and metallic nanoparticles for biomedical applications. Nanomed 2007; 2:287.
107. Liong M, Lu J, Kovochich M, et al. Multifunctional inorganic nanoparticles for imaging, targeting, and drug delivery. ACS Nano 2008;2:889.
108. Loo C, Lin A, Hirsch L, et al. Nanoshell-enabled photonics-based imaging and therapy of cancer. Technol Cancer Res Treat 2004;3:33.
109. Mulder WJ, Strijkers GJ, Habets JW, et al. MR molecular imaging and fluorescence microscopy for identification of activated tumor endothelium using a bimodal lipidic nanoparticle. Faseb J 2005;19:2008.
110. Saito R, Krauze MT, Bringas JR, et al. Gadolinium-loaded liposomes allow for real-time magnetic resonance imaging of convection-enhanced delivery in the primate brain. Exp Neurol 2005;196:381.
111. Caruthers SD, Wickline SA, Lanza GM. Nanotechnological applications in medicine. Curr Opin Biotechnol 2007;18:26.
112. Marsh JN, Partlow KC, Abendschein DR, et al. Molecular imaging with targeted perfluorocarbon nanoparticles: Quantification of the concentration dependence of contrast enhancement for binding to sparse cellular epitopes. Ultrasound Med Biol 2007;33:950.
113. Gillies ER, Frechet JMJ. Dendrimers and dendritic polymers in drug delivery. Drug Discov Today 2005;10:35.
114. Kobayashi H, Kawamoto S, Jo SK, et al. Macromolecular MRI contrast agents with small dendrimers: Pharmacokinetic differences between sizes and cores. Bioconjug Chem 2003;14:388.
115. Liu Z, Cai W, He L, et al. *In vivo* biodistribution and tumor targeting of carbon nanotubes in mice. Nature Nanotechnology 2007;2:47.
116. Keren S, Zavaleta C, Cheng Z, et al. Noninvasive molecular imaging of small living subjects using Raman spectroscopy. Proc Natl Acad Sci U S A 2008;105:5844.
117. Yu X, Munge B, Patel V, et al. Carbon nanotube amplification strategies for highly sensitive immunodetection of cancer biomarkers. J Am Chem Soc 2006;128:11199.
118. Shokeen M, Fettig NM, Rossin R. Synthesis, *in vitro* and *in vivo* evaluation of radiolabeled nanoparticles. Q J Nucl Med Mol Imaging 2008;52:267.
119. Pressly ED, Rossin R, Hagooly A, et al. Structural effects on the biodistribution and positron emission tomography (PET) imaging of well-defined (64)Cu-labeled nanoparticles comprised of amphiphilic block graft copolymers. Biomacromolecules 2007;8:3126.
120. Fukukawa K, Rossin R, Hagooly A, et al. Synthesis and characterization of core-shell star copolymers for *in vivo* PET imaging applications. Biomacromolecules 2008; 9:1329.
121. Sun X, Rossin R, Turner JL, et al. An assessment of the effects of shell cross-linked nanoparticle size, core composition, and surface PEGylation on *in vivo* biodistribution. Biomacromolecules 2005;6:2541.
122. Xu J, Sun G, Rossin R, et al. Labeling of polymer nanostructures for medical imaging: Importance of cross-linking extent, spacer length, and charge density. Macromolecules 2007;40:2971.
123. Cai W, Chen K, Li ZB, et al. Dual-function probe for PET and near-infrared fluorescence imaging of tumor vasculature. J Nucl Med 2007;48:1862.
124. Lee HY, Li Z, Chen K, et al. PET/MRI dual-modality tumor imaging using arginine-glycine-aspartic (RGD)-conjugated radiolabeled iron oxide nanoparticles. J Nucl Med 2008;49: 1371.

About the authors

Carolyn J. Anderson is a Professor of Radiology, Biochemistry, and Molecular Biophysics and Chemistry at Washington University in St. Louis. She received a B.S. degree in Chemistry from the University of Wisconsin–Superior in 1985 and a Ph.D. in Inorganic Chemistry from Florida State University in 1990. From 1990 to 1992, she was a postdoctoral research associate at the Mallinckrodt Institute of Radiology in the laboratory of Professor Michael J. Welch. In 1993, she was promoted to Assistant Professor of Radiology, and in 2007 she became full Professor of Radiology and Chemistry, followed by a joint appointment in Biochemistry and Molecular Biophysics in 2008. Professor Anderson's research interests involve the development of molecular imaging agents, primarily ^{64}Cu radiopharmaceuticals, for targeting cancer and cardiovascular disease. Her research group includes expertise in chelation and conjugation chemistry, as well as biologic evaluation of the molecular imaging agents in cell culture, preclinical animal models, and humans.

Riccardo Ferdani received his B.Sc. and Ph.D. degrees in Chemistry from the University of Parma (Italy) where he worked on calixarenes in the laboratories of Professors Rocco Ungaro and Andrea Pochini. In April 2000, he joined Professor George Gokel's group at Washington University School of Medicine (St. Louis, MO) and worked as a research associate on synthetic ion channels. In October 2006, he joined Professor Anderson's research group as a staff scientist at Washington University School of Medicine. His research interests focus mainly on synthesis and applications of macrocyclic chelators. He is currently working on the synthesis of novel cross-bridged azamacrocycles for facile, yet stable, chelation of ^{64}Cu for attachment to biologically targeted molecular-imaging agents.